WARSAW UNIVERSITY OF TECHNOLOGY Index 351733
FACULTY OF CIVIL ENGINEERING
COMMITTEE FOR CIVIL AND WATER ENGINEERING
POLISH ACADEMY OF SCIENCES ISSN 1230-2945

DOI: 10.24425/ace.2025.153332
ARCHIVES OF CIVIL ENGINEERING
Vol. LXXI ISSUE 1 2025
pp. 241 –257

Research paper

Validation of microplane coupled damage-plasticity model with gradient regularization (MCDPMwGR) on prestressed and non-prestressed concrete beams.

Damian Kowalski[1], Roman Gąćkowski[2], Jacek Selejdak[3]

Abstract: The paper aims validation of a microplane coupled damage-plasticity model with gradient regularization (MCDPMwGR) by simulating concrete behavior in reinforced concrete beams, both prestressed and non-prestressed. It uses experimental data from available papers. Tendons were modelled in a discrete form using one-dimensional finite elements. Prestress force was inflicted by a temperature drop. Contact issues were taken into account, i.e., friction and pressure at the interface between the cable and the duct wall. In the course of the work, it was found that it is possible to obtain satisfactory accuracy of results with the model in use. The adverse effects, present in other models were not observed. These are, among others, overestimate of ultimate load and excessive influence of tensile strength on the ultimate load value. We can observe such effects in plastic models (e.g., Menetrey–Willam or Drucker–Prager model) as well as non-coupled damage models (e.g., damage evolution model, microplane elastic model). Accurate $P - -\Delta$ (load-deflection) curves, matching with experimental data, were achieved. It is worth mentioning that the best curve fitting for beams made out of the same concrete was obtained using the same parameter values. This is true also when comparing prestressed and non-prestressed beams. It suggests significant potential of damage-plasticity model in predicting the true behavior of concrete. Yet, there are still some issues that need further analysis. They concern mainly influence of simplifications made during modelling prestressed beams on final results.

Keywords: concrete modelling, coupled damage-plasticity, microplane model, nonlinear analysis, numerical calculations, prestressed structures

[1]MSc., Eng., Częstochowa University of Technology, Faculty of Civil Engineering, Dąbrowskiego 69, 42-201 Częstochowa, Poland, e-mail: damian.kowalski@pcz.pl, ORCID: 0000-0002-0257-7642
[2]PhD., Eng., Częstochowa University of Technology, Faculty of Civil Engineering, Dąbrowskiego 69, 42-201 Częstochowa, Poland, e-mail: roman.gackowski@pcz.pl, ORCID: 0000-0002-4456-3011
[3]DSc., PhD., Eng., Częstochowa University of Technology, Faculty of Civil Engineering, Dąbrowskiego 69, 42-201 Częstochowa, Poland, e-mail: jacek.selejdak@pcz.pl, ORCID: 0000-0001-9854-5962

1. Introduction

With the advent of the era of numerical methods and the widespread use of computers, the possibilities of designing extremely complex structures have opened up for us. Optimization also took a prominent place in this process. However, it was paid for by the necessity of high specialization in the applied calculation methods. The multitude of available computational models and parameters, describing the behavior of materials, makes it necessary to perform a number of analyzes in order to find the optimal method of calculating various types of structures.

Searching of parameters values, which assure obtaining accurate $P - \Delta$ (load-deflection) curve, is, in fact, an optimization task, in which an objective function will be defined as a minimization of sum of differences between a force obtained in experimental and numerical analysis over the whole range of deflections. An equivalent to this, is an area between experimentally and numerically generated curves, calculated according to Eq. (1.1).

$$C = \int_0^{u_{\max}} |F_{\text{num}} - F_{\text{exp}}| \mathrm{d}u = \min \tag{1.1}$$

where: F_{num} – value of the force from numerical analysis, F_{exp} – force value measured during experiment, u – displacement of middle bottom of the beam.

Due to lack of smoothness of the $P - \Delta$ curve, the above integral could be determined only in finite number of discrete displacements. Therefore, only approximate fit can be achieved. The forces were subtracted in points of experimentally measured displacement, i.e. the forces associated with first crack, reinforcing steel yield, a maximum force and a force associated with the largest displacement.

Main motivation for this work was that authors could not find any publications on validation of microplane coupled damage-plasticity model with gradient regularization (MCDPMwGR) for numerical simulation of reinforced concrete beams, both prestressed and non-prestressed. Therefore, the aim of this paper was to validate that model. This was achieved by finding the results of the above stated optimization task. Experimental data used as a basis for the research and experiments themselves, were described in papers [1–3]. The test setup is shown in Fig. 1.

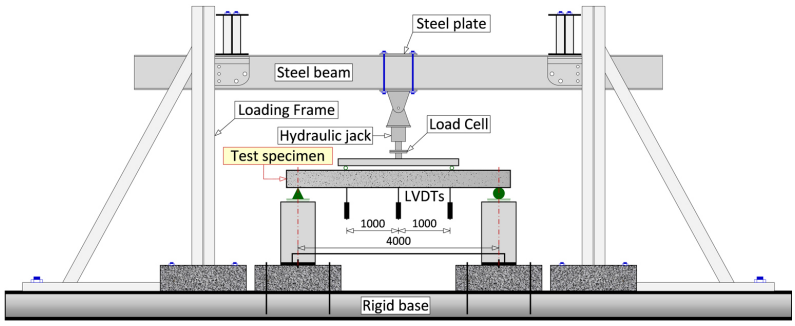

Fig. 1. Scheme of test set-up of beams B1 to B9

Figure 2 presents basic dimensions and boundary conditions of sample beams. As for prestressed beams, they included bonded and unbonded types of tendons. All the beams were subjected to 4-point bending. In this type of test, a middle part of the beam, located between the loads, is subjected to constant bending moment. Moreover, there is no shear along this section of the beam.

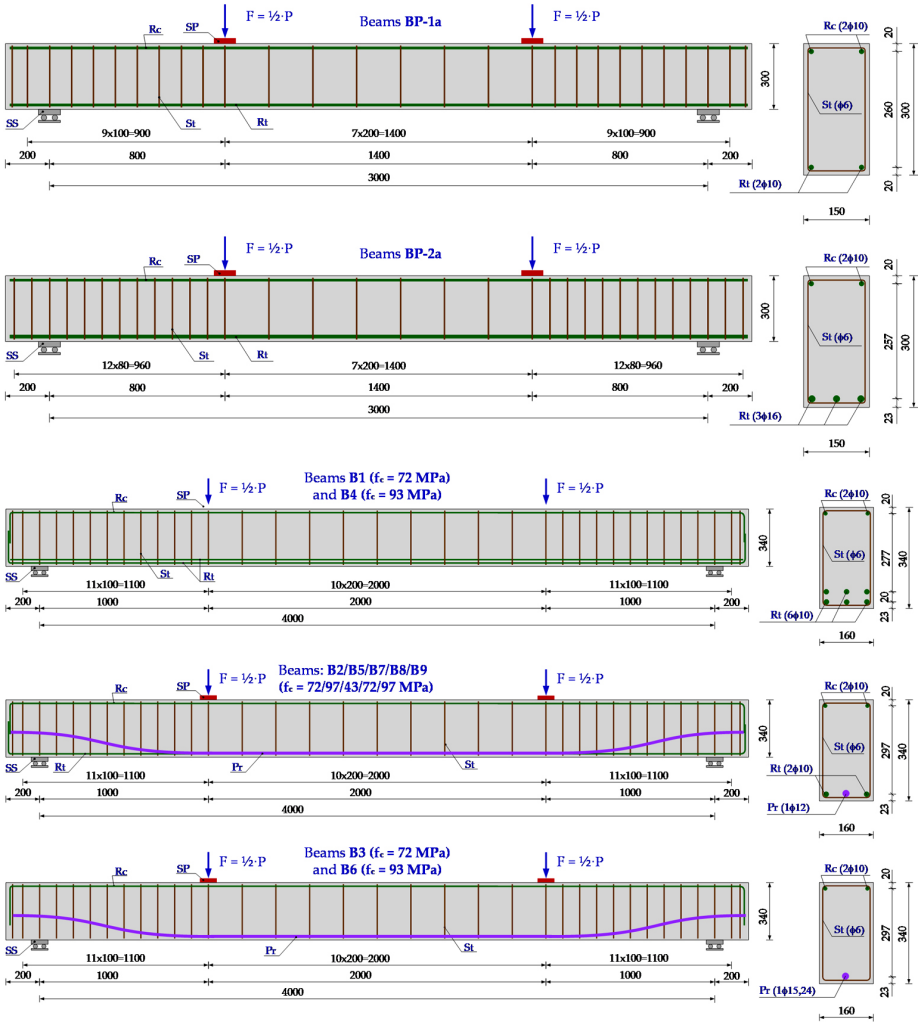

Fig. 2. Schemes of the analyzed beams

There are plenty of advanced software, both commercial and freeware. Abaqus seems to be one of the most poular amongst reinforced concrete structures researchers [4–6]. Yet, the new promising concrete model was recently implemented in Ansys program. Therefore the simulations were carried out using Ansys 2021 R2 edition. All the methods and parameters settings used during the research, are described in the following section.

2. Materials and methods

2.1. Concrete model

Precise modelling of concrete material is a difficult task, mainly due to complete difference in behavior of this material under compressive and tensile stresses. Moreover, unreinforced concrete is subject to brittle failure, which tends it to be described by means of the fracture mechanics [7]. The presence of reinforcement alleviates this restriction as a result of the increased ductility of the steel-concrete composite.

Concrete is also subject to rheological phenomena, which becomes particularly important in prestressed structures, as it affects the efficiency of prestressing [8].

In order to enable numerical simulations of concrete structures to be highly accurate in predicting the real behavior of structures, a number of advanced theoretical models of concrete were developed. There is a group of plastic models with strain softening effect included. Drucker–Prager [9, 10] and Menetrey–Willam [11, 12] can be mentioned here. Another type of models, that could be distinguished, describes material damage as a stiffness degradation related to stress or strain level. Examples of such formulation are damage evolution law [13] or elastic microplane model [14]. Due to omitting some essential features of brittle-plastic material, none of the above group gives satisfactory accuracy of results when it comes to concrete structures analysis. An ultimate load is significantly overestimated, furthermore, an influence of tensile strength on the ultimate load is considerable. Since tensile strength is usually determined as a derivative of compressive strength, the models listed above are impractical in experiment simulations field. Testing tensile strength is cumbersome and the results strongly depend on a way of proceeding the tests, therefore it is seldom performed.

Another group of material models worth mentioning is a group using fractional calculus in their constitutive relation [15, 16]. Generally, a non-integer order of derivative is used to express rate dependent plastic strains (viscosity) in visco-plastic formulations. Yet, the experiments analysed in this paper are quasi-static, therefore this group of material models seems to be too sophisticated to make use of them in this case.

The accuracy issues described above were solved in microplane coupled damage-plasticity model with implicit gradient regularization [17, 18]. It links the two salient aspects of concrete behavior: stiffness degradation with an increase of stresses and plastic strains persistence. Consequently, the accuracy of the obtained load-deflection dependency, is excellent. Moreover, the gradient regularization reduces solution sensitivity to finite element mesh.

The analyses were based on modified Drucker–Prager (D-P) model, already implemented in Ansys software, as Microplane Coupled Damage Plasticity Model with Gradient Regularization (MCDPMwGR). No additional changes were made to the originally defined model. A classic D-P is an elasto-plastic model, in which yield surface is defined in main stresses coordinate system (Fig. 3a). It accounts for differences in compression and tension strengths and an increase in strength of concrete, confined by compressive forces. In the modified D-P, the 3 yield surfaces (2 conical and one planar) were substituted by smooth surface, composed of one conical subsurface and 2 spherical surfaces, connected tangentially to the former (Fig. 3b). Thus, convergence problem in discontinuity regions of yield surface was eliminated.

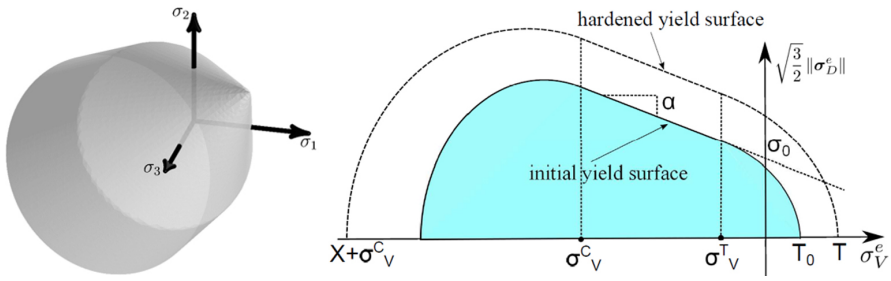

(a) (b)

Fig. 3. Yield surface in classic Drucker–Prager model (a) and a cross-section through the yield surface of the modified Drucker–Prager model (b)

Elastic modulus (E_{cm}) of beams tested in [1] was taken the same as in the paper, i.e. for beam BP-1a – 36.8 GPa and for beam BP-2a – 36.4 GPa, whereas for beams described in [3] (beams B1 to B9), due to lack of data, the Young's modulus was calculated according to [8]. The uniaxial tensile strength (f_{ut}) was assumed an optimization parameter. Poisson ratio (ν) of uncracked concrete has been adopted from source papers, i.e., 0.15 for beams BP-1a and BP-2a [1] and 0.2 for beams B1-B9 [3]. Biaxial compressive strength (f_{bc}) was taken, following [19, 20], as 1.15 of uniaxial compressive strength:

$$f_{bc} = 1.15 f_{uc} \tag{2.1}$$

where: f_{uc} – uniaxial compressive strength of concrete.

For the σ_V^C parameter (i.e., intersection point abscissa between compression cap and Drucker–Prager yield function), an approximate formula has been used:

$$\sigma_V^C \approx -\frac{2}{3} f_{bc} \tag{2.2}$$

where: f_{bc} – biaxial compressive strength of concrete.

The basic concrete characteristics are set together in Table 1.

Some model parameters were assumed constant, since their influence, confirmed in sensitivity analysis proceeded by authors, is negligible. These are the following parameters and their value used through all analyses:

- Over-nonlocal averaging parameter: $m = 2, 5$,
- Tension damage threshold: $\gamma_{t0} = 0$,
- Compression damage threshold: $\gamma_{c0} = 0$,
- Tension cap hardening constant: $R_T = 1$,
- Ratio between the major and minor axes of the cap: $R = 1$,
- Hardening material constant: $D = 0$.

Concrete matrix has been modelled by means of 8-node hexahedron shaped solid finite elements, having 3 degrees of freedom in each node. Size of elements ranging between 20 and 80 millimeters. Gradient regularization method used here [17, 18] required a definition of 2 additional degrees of freedom in each node. Sample cross-section through prestressed beam

Table 1. Basic concrete parameters

Sample	Young's modulus, E_{cm}, GPa	Uniaxial compressive strength, f_{uc}, MPa	Biaxial compressive strength, f_{bc}, MPa	Poisson's ratio, ν	Intersection point abscissa between compression cap and Drucker–Prager yield function, σ_V^C, MPa
BP-1a	36.8	81.2	93.4	0.15	–62.3
BP-2a	36.4	78.8	90.6	0.15	–60.4
B1	39.78	72	82.8	0.2	–55.2
B2	40.27	75	86.25	0.2	–57.5
B3	40.43	76	87.4	0.2	–58.3
B4	43.23	95	109.25	0.2	–72.8
B5	43.50	97	111.55	0.2	–74.4
B6	43.09	94	108.1	0.2	–72.1
B7	34.08	43	49.45	0.2	–33.0
B8	39.78	72	82.8	0.2	–55.2
B9	43.23	95	109.25	0.2	–72.8

with unbonded tendon is shown in Fig. 4. Due to symmetry, only half of the beam (cut in the middle of its length) is modelled. In case of prestressed structures, it is sensible to simplify the model this way only when the prestress force is applied at both ends. Otherwise, there is no symmetry in real tendon behavior.

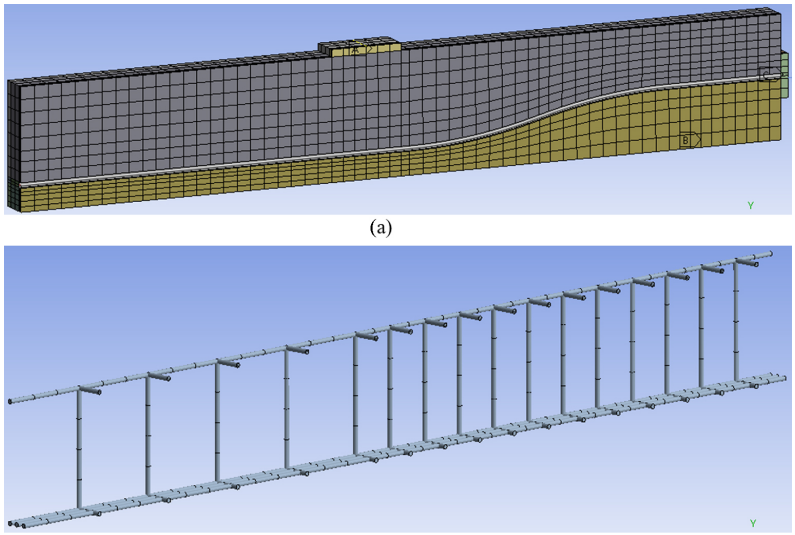

(a)

(b)

Fig. 4. Cross-section through model of prestressed concrete beam with unbonded tendons (a) and passive reinforcement model (b)

2.2. Prestressing tendons model

Prestressing tendons were modelled by means of 1-dimensional, 2-node finite elements, with 7 degrees of freedom per node, i.e., 3 translational, 3 rotational and 1 torsional. They are based on Timoshenko's theory, which includes shear deformations. The tendons are anchored at the ends of the beams, in steel plates, which, in turn, are permanently connected with the adjacent concrete (see Fig. 4a).

A bilinear model of material, elasto-plastic, with kinematic hardening, was adopted. In this model, the first segment of the σ-ε (stress-strain) curve stays in the elastic range, and the remaining ones represent this relationship after yielding. The kinematic strengthening reflects the increase in the yield point due to plasticity in tension, while reducing it at the same time under compression (Bauschinger effect).

The yield point of the tendons (f_{yk}), according to [3], is 1674 MPa. The modulus of elasticity in the elastic strains range, was assumed to be 195 GPa. It is worth mentioning that in the triaxial stress / strain state, this modulus refers to the values of reduced stresses and strains. The stiffness modulus after yielding was obtained from:

$$E_T = \frac{f_{ut} - f_{yk}}{\varepsilon_{uk} - \varepsilon_{yk}} \tag{2.3}$$

where: E_T – modulus of plastic strain of reinforcement steel, f_{ut} – uniaxial tensile strength of reinforcement, f_{yk} – characteristic yield strength of reinforcement, ε_{uk} – characteristic strain of reinforcement or prestressing steel at maximum load, ε_{yk} – strain of reinforcing steel at which the steel reaches the yield strength.

The prestress in the cables was given in the form of a temperature drop, according to the formula:

$$\Delta t = -\frac{F}{\alpha E A} \tag{2.4}$$

where: Δt – temperature drop in the cables during prestressing, F – prestressing force, α – thermal expansion coefficient, E – Young's modulus, A – cable cross-sectional area.

The prestressing force is taken directly from experiments, where it was given after losses. It should be emphasized that the prestress losses were not modelled explicitly. Therefore effects such as non-uniform distribution of losses, were not taken into account. Important part of prestress losses in post-tensioned elements is caused by the anchorage slip. These losses may concentrate in the neighborhood of anchorages due to channel track deflection. This is the potential source of discrepancies.

The beams with unbonded tendons were assumed to fill a channel of diameter 4 mm greater than the tendon diameter. Frictional contact type was applied at the interface between 1-dimensional tendon representation (Edge) and surface of the channel (Face). CONTAC175 and TARGE170 elements were utilized to simulate contact conditions. A static friction coefficient became an optimization parameter. Table 2 shows the properties of prestress, as presented in the original papers [1–3]. The prestressing force was measured at the anchorage.

Table 2. Steel parameters

Sample	Yield strength of steel passive reinforcement, f_{yk}, MPa	Tangent modulus of passive / prestressing reinforcement, E_T, GPa	Type of longitudinal reinforcement	Tendons cross-sectional area, A, mm^2	Elongation after friction losses, ΔL, mm	Measured prestressing force, F, kN
BP-1a	420	1.96 / –	P	–	–	–
BP-2a	437	2.66 / –	P	–	–	–
B1	470	1.93 / –	P	–	–	–
B2	470	1.93 / 4.47	P + BT	99	22.22	100
B3	470	– / 4.47	BT	140	22.06	140
B4	470	1.93 / –	P	–	–	–
B5	470	1.93 / 4.47	P + BT	99	22.58	102
B6	470	– / 4.47	BT	140	22.15	142
B7	470	1.93 / 4.47	P + UT	99	23.02	104
B8	470	1.93 / 4.47	P + UT	99	22.3	101
B9	470	1.93 / 4.47	P + UT	99	22.93	104

where: P – passive reinforcement, BT – bonded tendons, UT – unbonded tendons.

2.3. Non-prestressed reinforcement model

Model of passive reinforcement used 1-dimensional, 2-node finite elements, with 1 degree of freedom per node, accounting for longitudinal stiffness only. Material model was assumed analogously to prestressed steel – bilinear with kinematic hardening. Young's modulus was taken as 205 GPa, and Poisson ratio – same as for tendons – 0.3. A yield strength is shown in Table 2. Perfect bond between passive reinforcement and concrete matrix was assumed. It was implemented by direct node merge. According to other studies [21], bond-slip characteristics of reinforced concrete have little effect on the load-deflection characteristics.

2.4. Other model properties

Calculations were performed using the full Newton-Raphson method, in which the stiffness matrix is updated at every equilibrium iteration. In addition, it generated and used unsymmetrical matrices. Non-linear stabilization of the stiffness matrix was also utilized to ease the process convergence. Force convergence limit was set to 5×10^{-5} N and a moment convergence was set to 0.05 N·mm. A detailed analysis of reinforced concrete structures required the formulation of large displacements. Moreover, in order to perform the calculations efficiently, a non-symmetric solver was used, which copes well with difficulties related with

numerical process convergence during the analysis of brittle materials. Quasi-static approach also helped obtaining convergence. Its assumptions are true for systems changing slowly. Furthermore, a more stable numerical process was obtained by using the tangential elastic matrix of the material instead of the consistent matrix. The calculations were controlled by means of displacement increase.

Analyses were carried on workstation with 32 core CPU, able to work with frequency up to 4.5 GHz, having 64 GB of Random Access Memory and Solid-State Disc with sequential read / write top speed reaching 14 and 10.4 GB/s.

2.5. Optimization procedure

Firstly, the model parameters, which influence the results, were identified. Then, broad ranges of values for these parameters were assumed. Each range was divided into many equal subsets, from which one representative value was taken. Each combination of these values was used to calculate one instance of the model. This allowed narrowing these ranges down to extent, for which convergence was obtained and a final beam deflection was achieved. Next, the new ranges were divided into finer sections with their new representative values. Then the analyses were executed again for each combination of these values. For each analysis, a sum of differences between the force yielded in the experiment and as a result of calculations, was determined. Since exact values of the force from experiment are known in specific points, only these values were taken into account. These are the forces associated with first crack, reinforcing steel yield, a maximum force and a force associated with the largest displacement. At last, a set of parameters associated with the smallest sum was chosen as the optimal set.

3. Results

The optimization results are the model parameters values, given in Table 3. These values minimize objective function, interpreted as the area between experimental and numerical P–Δ curve. Since the uniaxial tensile strength was not measured during experiments, it is treated as an optimization parameter. Therefore, the optimal value of this parameter, just as the other optimal parameter values, ensures the best fit of P–Δ curves.

Table 3. Optimal parameter values

Sample	**Uniaxial tensile strength of concrete, f_{ut}, MPa**	**Nonlocal interaction range parameter, c, mm^2**	**Tensile damage evolution constant, β_t**	**Compressive damage evolution constant, β_c**	**Static friction coefficient between tendon and concrete, μ**
BP-1a	2	5 000	5 000	0	–
BP-2a	2	5 000	5 000	0	–

Continued on next page

Table 3 – *Continued from previous page*

Sample	**Uniaxial tensile strength of concrete, f_{ut}, MPa**	**Nonlocal interaction range parameter, c, mm^2**	**Tensile damage evolution constant, β_t**	**Compressive damage evolution constant, β_c**	**Static friction coefficient between tendon and concrete, μ**
B1	3.5	28 000	20 000	1 000	–
B2	3.5	28 000	20 000	1 000	–
B3	3.5	28 000	20 000	1 000	–
B4	3.5	28 000	20 000	1 000	–
B5	3.5	28 000	20 000	1 000	–
B6	3.5	28 000	20 000	1 000	–
B7	2.5	28 000	250	0	10
B8	3.5	28 000	20 000	1 000	1.5
B9	3.5	28 000	20 000	1 000	6

Table 4 gathers values of forces and displacements for all tested beams. These values correspond to the moment of first crack formation, steel yielding and reaching ultimate load. Numerical model values were read based on stresses averaged over each finite element.

Table 4. Main experimental and numerical results

Sample	**Source of results**	**P_{cr}, kN**	**Δ_{cr}, mm**	**P_y, kN**	**Δ_y, mm**	**P_{max}, kN**	**Δ at P_{max}, mm**	**Δ_{max}, mm**
BP-1a	experiment	–	–	–	–	30	180	180
	model	11.2	1.3	22	10.1	30.2	175	175
BP-2a	experiment	–	–	–	–	105	111	111
	model	15.4	1.35	78.8	14	102.8	143	143
B1	experiment	33	2.54	103	16.8	152	141	141
	model	32	2.2	136.8	21.5	149.6	99	99
B2	experiment	64	3.15	79	19.1	148	122	151
	model	49	1.4	124	29.4	146	109	158

Continued on next page

Table 4 – *Continued from previous page*

Sample	Source of results	P_{cr}, kN	Δ_{cr}, mm	P_y, kN	Δ_y, mm	P_{max}, kN	Δ at P_{max}, mm	Δ_{max}, mm
B3	experiment	70	3.57	83	19.9	135	63	63
	model	69	1.9	104.4	15.4	139.5	111	156
B4	experiment	39	2.81	105	18.9	157	138	152
	model	35	1.6	136	21	155	190	195
B5	experiment	67	3.56	81	19.8	153	112	121
	model	63.6	2	80	9.4	150	121	121
B6	experiment	74	4.09	88	20.7	145	76	102
	model	70.4	1.9	103.2	14.1	143	138	138
B7	experiment	47	4.07	115	29.2	141	76	91
	model	29.4	1.2	103.6	19.7	140	67.6	99.6
B8	experiment	63	3.54	113	25.4	148	66	76
	model	43.4	1.3	106.6	20	146	92	92
B9	experiment	65	3.6	121	24.8	155	53	70
	model	56.8	1.7	119.2	19.1	150.4	91.5	91.5

where: P_{cr} – load corresponding to first crack formation, Δ_{cr} – displacement corresponding to first crack formation, P_y – load and displacement corresponding to passive reinforcement yielding, Δ_y – displacement corresponding to passive reinforcement yielding, P_{max} – ultimate load, Δ at P_{max} – displacement corresponding to ultimate load, Δ_{max} – maximum displacement.

Figure 5 shows comparison of load-deflection curves between experiment and optimal numerical simulation. Beginning and end part of P–Δ curves of beam BP-1a fit accurately. The difference arises in the section right after concrete cracking, where calculated curve is placed below experimentally obtained. A maximum difference in load is 1.2 kN (that is 4.5% of experimental value) and it corresponds to displacement of 53 mm. The charts associated with BP-2a beam show biggest discrepancy at end section, that is in the ultimate load area. This discrepancy reaches 4.7 kN (4.5% of experimental value) for ultimate displacement being 100 mm. The diversity of ordinates of B1 beam does not exceed 4.3 kN (3% of experimental value). The top difference occurs at 84 mm displacement. B2 curves are virtually coincident over the entire length. The biggest deviation was noticed at the end of curves, which is 133 mm. It's been 4.6 kN, making it 3% of the experimental value. The highest differences for other

beams are: in B3 beam – 4.7 kN (3.5% of experimental load) at 61.5 mm; B4 – 17.2 kN (16.4%) at 18.5 mm; B5 – 8 kN (5.4%) at 44 mm; B6 – 6.3 kN (4.6%) at maximum displacement, i.e. 101 mm; B7 – 4.3 kN (3.2%) also at top displacement, which is 91 mm; B8 – 3.5 kN (2.4%) at 66 mm; B9 – 9.3 kN (6.7%) at top displacement = 69 mm.

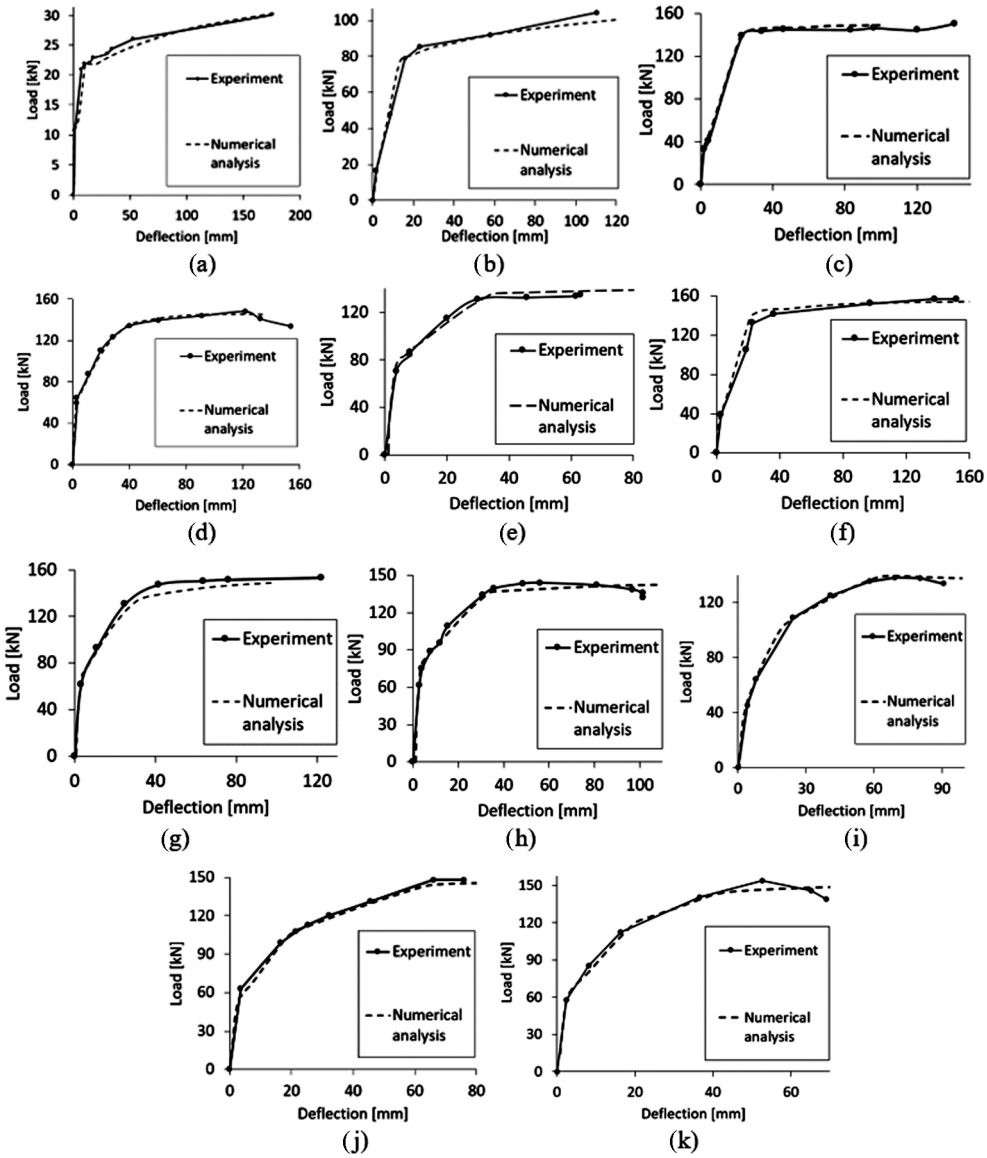

Fig. 5. Comparison of numerical and experimental load-deflection curves of beams BP-1a (a), BP-2a (b), B1 (c), B2 (d), B3 (e), B4 (f), B5 (g), B6 (h), B7 (i), B8 (j) and B9 (k)

Figure 6 presents exemplary stress maps of reinforcement, corresponding to ultimate load. Yielding of bottom bars of passive reinforcement (Fig. 6a and 6b) and prestressing tendon (Fig. 6b) can be observed.

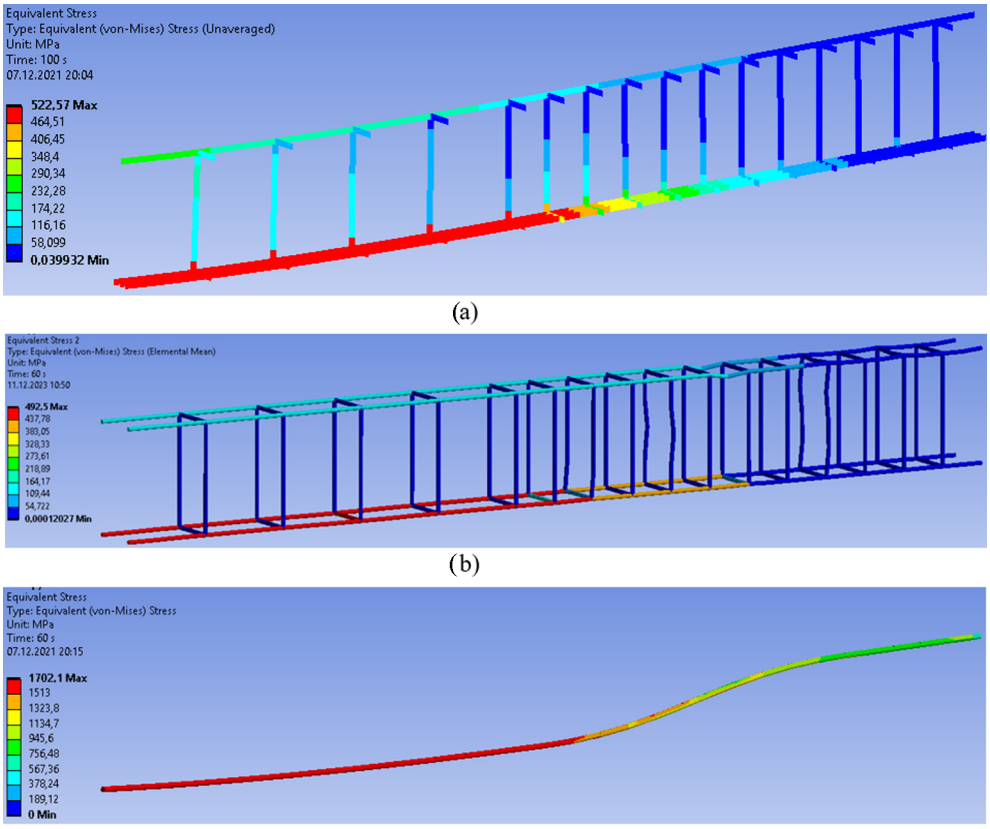

Fig. 6. Final stresses in passive reinforcement of B1 beam (a), B8 beam (b) and in prestressed tendon of B8 beam (c)

4. Discussion

The differences between experimental and numerical curves do not exceed 5%, except one case, where the difference was 16,5%. Exact values are provided in chapter 3. Taking account of highly nonlinear concrete behavior and a variety of phenomena present in this material, these differences may be classified as acceptable.

The obtained nonlocal parameter c value is very high. This parameter is associated with nonlocal effects such as macro-crack, forming in concrete. With such a value of this parameter

it is impossible to generate realistic cracks distribution. According to [22], nonlocal parameter is directly associated with maximum aggregate size and can be approximated by formula:

$$c \cong (2,7d)^2 \tag{4.1}$$

where: d – aggregate size.

Another parameter requiring detailed analysis is friction coefficient between concrete and tendons. Though existing of friction coefficient greater than 1 is not to be excluded in real world, yet obtained values are much too high. If the tendons are covered with HDPE coat then the friction coefficient according to [23] should stay within range 0.05–0.07. For tendons without the coat, the friction coefficient between steel and concrete, according to table 5.1 of [8], should have a value between 0.19 and 0.65. The reason for this discrepancy could be a simplification of using 1-dimensional finite elements to represent tendons. This approach seems to be accurate enough only, if no contact-associated phenomena are to be analyzed.

Best curves fit was achieved for tensile strength lower than commonly taken [8]. For instance, a concrete having compressive strength of 43 MPa, has, according to mentioned standard, 4.13 MPa of tensile strength, while best curves fit is provided by 2.5 MPa. Concretes with f_{uc} equal 72 and 95 MPa and code tensile strength, respectively, 4.46 and 4.98 MPa, will yield the most accurate results using 3.5 MPa value. It is worth noticing that all the optimizations yielded lower tensile strength than the code values.

5. Conclusions

The aim of analyses covered by this paper was finding microplane coupled damage-plasticity model with gradient regularization (MCDPMwGR) parameters, yielding best fit of experimental and numerical load-deflection curves. The investigated parameters were microplane damage-plasticity concrete model parameters as well as the tensile strength of concrete and the friction coefficient between concrete and tendon in beams prestressed with unbonded tendons.

The above task is an optimization problem, where the objective function can be defined as minimization of sum of differences between a force obtained in experimental and numerical analysis over the whole range of deflections. An equivalent to this, is an area between experimentally and numerically generated curves.

The target was reached numerically with satisfactory result, nevertheless optimal parameters values obtained require further, more detailed analyses. High value of nonlocal parameter c did not let achieving the realistic macrocracks distribution. On the other hand, lower values of c parameter did not let the most accurate $P - \Delta$ curves fit.

High values of c and β_t parameters may indicate a salient influence of a method and conditions of proceeding the experiments. The difference between values of these parameters from one experiment set to another (made in different laboratory by different researchers) seems to confirm that presumption.

Moreover, the best curves fit in prestressed beams with unbonded tendons, was possible to yield using only high values of friction coefficient between the tendon and surrounding concrete.

This could happen due to simplified tendons modelling, by means of 1-dimensional finite elements and/or simplified prestress force modelling by uniform temperature drop along the whole tendon. It does not take the non-uniform prestress losses distribution into account. This way of modelling should therefore be deemed too simplified. Authors' future plans cover research of more accurate ways of tendons modelling, but this requires more computational power.

The adverse effects observed in pure plastic models (e.g., Menetrey–Willam, classic Drucker–Prager) and pure damage models (e.g., damage evolution model, microplane elastic model) are not noticed here. These are, among others, overestimate ultimate load and excessive sensitivity of the ultimate load to uniaxial tensile strength of concrete.

Properly calibrated damage-plasticity concrete model allows for satisfactory accurate simulation of concrete beams, passively reinforced and prestressed with bonded tendons. Due to high values of obtained friction coefficient for beams prestressed with unbonded tendons, this type of structures needs further investigation, since such values of this coefficient might be a result of excessive simplification. There are some other issues to investigate as well. Particularly, the finite element mesh density influence on optimal model parameters, especially c and β_t. Also, justification of using simplified tendons modelling, using 1-dimensional finite elements.

References

[1] P. Smarzewski, *Modelowanie statycznego zachowania niespre?zÿystych belek zÿelbetowych wykonanych z betonu wysokiej wytrzymałosìc*. Lublin: Politechnika Lubelska, 2011.

[2] P. Smarzewski and A. Stolarski, "Numerical analysis on the high-strength concrete beams ultimate behaviour", *IOP Conference Series: Materials Science and Engineering*, vol. 245, no. 3, 2017, doi: 10.1088/1757-899X/245/3/032013.

[3] O.F. Hussien, T.H.K. Elafandy, A.A. Abdelrahman, S.A. Abdel Baky, and E.A. Nasr, "Behavior of bonded and unbonded prestressed normal and high strength concrete beams", *Housing and Building National Research Center Journal*, vol. 8, no. 3, pp. 239–251, 2012, doi: 10.1016/j.hbrcj.2012.10.008.

[4] N. Staszak, T. Garbowski, and B. Ksit, "Application of the generalized nonlinear constitutive law in numerical analysis of hollow-core slabs", *Archives of Civil Engineering*, vol. 68, no. 2, pp. 125–145, 2022, doi: 10.24425/ace.2022.140633.

[5] N.A.M. Mortar, et al., "Finite element analysis on structural behaviour of geopolymer reinforced concrete beam using Johnson-Cook Damage in Abaqus", *Archives of Metallurgy and Materials*, vol. 67, no. 4, pp. 1349–1354, 2022, doi: 10.24425/amm.2022.141061.

[6] M. Cwyl, S. Wierzbicki, and R. Michalczyk, "Laboratory tests and numerical analysis of façade substructure made of austenitic steel", *Archives of Civil Engineering*, vol. 68, no. 4, pp. 237–252, 2022, doi: 10.24425/ace.2022.143036.

[7] S.P. Shah, "Determination of fracture parameters (KsIC and CTODc) of plain concrete using three-point bend tests", *Materials and Structures*, vol. 23, no. 6, pp. 457–460, 1990, doi: 10.1007/BF02472029.

[8] EN 1992-1-1:2004 Eurocode 2: Design of concrete structures - Part 1-1: General rules and rules for buildings. CEN, 2004.

[9] L.R. Alejano and A. Bobet, "Drucker–Prager criterion", *Rock Mechanics and Rock Engineering*, vol. 45, no. 6, pp. 995–999, 2012, doi: 10.1007/s00603-012-0278-2.

[10] T. Yu, J.G. Teng, Y.L. Wong, and S.L. Dong, "Assessment of drucker-prager type plasticity models for predicting the behaviour of FRP-confined concrete", in *Proceedings of the First Asia-PacificConference on FRP in Structures*, S. T. Smith, Ed. Hong Kong: International Institute for FRP in Construction, 2007, pp. 161–166. [Online]. Available: https://ro.uow.edu.au/eispapers/559/.

[11] A.A. Pisano, "An algorithmic approach for peak load evaluation of structural elements obeying a Menetrey–Willam type yield criterion", *Electronic Journal of Differential Equations*, vol. 167, pp. 1–9, 2012.

[12] A.A. Pisano, P. Fuschi, and D. De Domenico, "Peak load computation of 3D concrete elements by Menétrey-Willam pressure sensitive yield condition", in *Conference: Atti del XIX Convegno Italiano di Meccanica Computazionale GIMC2012*, 2012. [Online]. Available: https://www.researchgate.net/publication/267379171.

[13] P. Kral, P. Hradil, J. Kala, F. Hokes, and M. Husek, "Identification of the parameters of a concrete damage material model", *Procedia Engineering*, vol. 172, pp. 578–585, 2017, doi: 10.1016/j.proeng.2017.02.068.

[14] I. Carol and P.C. Pratt, "New explicit microplane model for concrete : theoretical aspects and numerical implementation", *International Journal of Solids and Structures*, vol. 29, no. 9, pp. 1173–1191, 1992, doi: 10.1016/0020-7683(92)90141-F.

[15] W. Sumelka, et al., "Dynamic failure of the aluminium plate under air-blast loading in the framework of the fractional viscoplasticity model - theory and validation", *International Journal of Impact Engineering*, vol. 158, 2021, doi: 10.1016/j.ijimpeng.2021.104024.

[16] W. Sumelka, "Fractional viscoplasticity", *Mechanics Research Communications*, vol. 56, pp. 31–36, 2014, doi: 10.1016/j.mechrescom.2013.11.005.

[17] I. Zreid and M. Kaliske, "A gradient enhanced plasticity–damage microplane model for concrete", *Computational Mechanics*, vol. 62, no. 5, pp. 1239–1257, 2018, doi: 10.1007/s00466-018-1561-1.

[18] I. Zreid and M. Kaliske, "A cyclic triaxial concrete microplane model with gradient regularization", in *Computational Modelling of Concrete Structures*, G. Meschke, B. Pichler, and J. G. Rots, Eds. London: Taylor & Francis Group, 2018, pp. 413–420.

[19] H. Kupfer, H.K. Hilsdorf, and H. Rusch, "Behavior of Concrete Under Biaxial Stresses", *ACI Journal*, vol. 66, pp. 656–666, 1969.

[20] J. Lubliner, J. Oliver, S. Oller, and E. Oñate, "A plastic-damage model for concrete", *International Journal of Solids and Structures*, vol. 25, no. 3, pp. 299–326, 1989.

[21] S. Wang and D. Wang, "A study on the deflection and crack layout in a hollow slab bridge", *Archives of Civil Engineering*, vol. 69, no. 3, pp. 541–555, 2023, doi: 10.24425/ace.2023.146096.

[22] Z.P. Bazant and G. Pijaudier-Cabot, "Measurement of characteristic length of nonlocal continuum", *Journal of Engineering Mechanics*, vol. 115, no. 4, pp. 755–767, 1989.

[23] Model Code 2010 : First complete draft. International Federation for Structural Concrete, 2010.

[24] E.A. Hansen, "Determination of the tensile strength of concrete", *Nordic Concrete Research-Publications*, vol. 17, pp. 1–17, 1995.

[25] M. Ahmed, J. Mallick, and M. Abul Hasan, "A study of factors affecting the flexural tensile strength of concrete", *Journal of King Saud University - Engineering Sciences*, vol. 28, no. 2, pp. 147–156, 2016, doi: 10.1016/j.jksues.2014.04.001.

Walidacja modelu mikropłaszczyznowego sprzężonego uszkodzeniowo-plastycznego z regularyzacją gradientową (MCDPMwGR) na belkach betonowych sprężanych i niesprężanych

Słowa kluczowe: analiza nieliniowa, konstrukcje sprężone, model mikropłaszczyznowy, modelowanie betonu, obliczenia numeryczne, sprzężenie uszkodzeniowo-plastyczne

Streszczenie:

Celem pracy jest walidacja modelu mikropłaszczyznowego sprzężonego uszkodzeniowo-plastycznego z regularyzacją gradientową (MCDPMwGR) poprzez symulację zachowania betonu w belkach żelbetowych, zarówno sprężonych, jak i niesprężonych. Wykorzystano dane eksperymentalne z dostępnych publikacji. Cięgna zamodelowano w postaci dyskretnej, przy użyciu jednowymiarowych elementów skończonych. Siła sprężająca była modelowana spadkiem temperatury. Uwzględniono kwestie styku, czyli tarcia i docisku na styku kabla ze ścianą kanału. W toku prac stwierdzono, że przy zastosowanym

modelu możliwe jest uzyskanie zadowalającej dokładności wyników. Nie zaobserwowano negatywnych skutków występujących w innych modelach. Są to między innymi: przeszacowanie obciążenia granicznego oraz nadmierny wpływ wytrzymałości na rozciąganie na wartość obciążenia niszczącego. Efekty takie możemy zaobserwować w modelach plastycznych (np. model Menetreya–Willama czy Druckera–Pragera) oraz w modelach uszkodzeniowych niesprzężonych (np. model ewolucji uszkodzeń, model mikropłaszczyznowy sprężysty). Uzyskano dokładne krzywe P–Δ (odkształcenie obciążenia), zgodne z danymi eksperymentalnymi. Warto wspomnieć, że najlepsze dopasowanie krzywej dla belek wykonanych z tego samego betonu uzyskano przy zastosowaniu tych samych wartości parametrów. Dotyczy to również porównania belek sprężonych i niesprężonych. Sugeruje to znaczny potencjał modelu uszkodzeniowo-plastycznego w przewidywaniu prawdziwego zachowania betonu. Jednakże nadal istnieją pewne kwestie wymagające dalszej analizy. Dotyczą one głównie wpływu uproszczeń dokonanych podczas modelowania belek sprężonych na wyniki końcowe.

Received: 2023-08-29, Revised: 2024-03-19